Adsorption (2013) 19:835–840
DOI 10.1007/s10450-013-9526-3

Direct contact free real-time acquisition of temperature profiles in adsorbent bed during vacuum swing adsorption

Maxim S. Mel'gunov · Artem B. Ayupov · Vladimir B. Fenelonov · Boris G. Vainer

Received: 1 November 2012 / Accepted: 18 February 2013 / Published online: 29 March 2013

Abstract Real-time temperature co-axial profiles in a bed of mesoporous alumosilicate were recorded by means of FPA-based infrared thermography during air drying vacuum swing adsorption cycles. The good correlation between experimentally measured temperature profiles and profiles simulated on the basis of linear driving force model of mass and heat transfer in nonadiabatic regime is observed.

Keywords Non-isothermal adsorption · Vacuum swing adsorption · FPA-based infrared thermography · Temperature profiles

IR Infra red
PSA Pressure swing adsorption
VSA Vacuum swing adsorption

The research was supported by the Russian Foundation for Basic Research (grant No. 11-03-00900).

M. S. Mel'gunov (✉) · A. B. Ayupov · V. B. Fenelonov
G.K.Boreskov Institute of Catalysis, Siberian Branch of the Russian Academy of Sciences, 5 Lavrentyev av, Novosibirsk 630090, Russia
e-mail: 2max@bk.ru; max@catalysis.ru
URL: http://www.nsu.ru

M. S. Mel'gunov · V. B. Fenelonov · B. G. Vainer
Novosibirsk State University, 2 Pirogova, Novosibirsk 630090, Russia
e-mail: BGV@isp.nsc.ru

B. G. Vainer
A.V.Rzhanov Institute of Semiconductor Physics, Siberian Branch of the Russian Academy of Sciences, 13 Lavrentyev av, Novosibirsk 630090, Russia

1 Introduction

Processes of pressure or vacuum swing adsorption (PSA or VSA) have taken a special niche in modern separation of gas mixtures (Ruthven et al. 1994; Voss 2005; Wilcox 2012). The possibility to apply these processes in practice is based on a number of requirements, including maintenance of relatively low cost of separated mixtures, application of adsorbents that are capable of adsorbing different components depending on the separation mode (equilibrium, kinetic or "steric" modes), etc. The flow rate of feeding gas is varied in a range of 10^{-1}–200 m^3/h usually. Membranes are more cost-effective at lower flow rates, and cryogenic separation methods are usually applied at larger flow rates. In a PSA process it is common that the part of the product gas is "lost" due to the necessity to regenerate the adsorbent under reduced pressure to provide the next cycle. This gas can be recycled, but it is often not cost effective. To reduce the losses associated with regeneration, the multi-bed PSA setups are constructed. In such cases the regeneration is divided into several stages and, conditionally, the same amount of gas is spent on the regeneration of not one, but several adsorption layers. Therefore PSA processes are not widely used in the separation of, for example, hydrocarbons in the chemical industry due to both economic and environmental reasons, because the loss of a part of product gas is unacceptable. The most widely used PSA and VSA processes are applied to the separation of air for small enterprises, medical and household purpose, drying, removal of CO_2 and other harmful air contaminants. The only large-scale PSA process is the production of hydrogen from the synthesis gas (Guerrero-Lemus and Martinez-Duart 2013) and, it seems, that this is the only mixture for which a single pass provides the concentration of hydrogen to a very high purity

(up to 99.9999+ %) with losses for the regeneration of no more than 15–20 %.

Complexity of modern multi-bed PSA systems requires the use of advanced predictive models that include the consideration of both co-axial and radial mass and heat transfer, non-isothermal regime, diffusion in the bed and in the adsorbent (Khalighi et al. 2012). Usually the parameters for modeling and verification of models are provided using relatively simple adsorption experiments, such as PSA or VSA in a single tubular layer of adsorbent granules. The main verification parameter is the so-called breakthrough concentration curve, which represents the time dependence of the components concentration at the outlet of the adsorbent bed. Verification of the distribution of heat in the adsorption layer is usually not carried out due to the experimental difficulties of measuring the temperature profiles in the bed. However, the heating and cooling of the adsorbent as a result of adsorption–desorption processes can be significant and, more important, the process itself can be non-stationary during a long period of time, which depends on the efficiency of heat exchange with the ambient. It is known that the thermal conditions of the adsorber (adiabatic/non-adiabatic) have a significant influence on the separation efficiency. In modern literature, there is a clear lack of information on the distribution of heat in adsorption beds during PSA cycles that can be used for a verification of the developed models. Previously, to obtain temperature profiles, one installed a set of temperature sensors inside a bed through the side walls of absorbers (Lou et al. 1999). However, this method cannot be considered as completely reliable, because "alien" perturbations in the bed can uncontrollably affect the heat and mass transfer.

However, there is a fairly simple method to obtain such information: the infrared thermography (IRT). This method has recently became frequently used in a number of scientific, technical and biomedical applications. In particular, it is known to be used for specific tasks in the field of catalysis and gas adsorption (Loskyll et al. 2012; Jolly et al. 2011; Vainer et al. 2011, 2012; Berkessel et al. 2003). The most advanced version of this method is based on the use of infrared cameras equipped with focal-plane array (FPA)-based infrared detectors.

The purpose of this work is to demonstrate the potential of modern FPA-based IRT method in the field of gas separations by means of PSA and VSA.

2 Experimental

Mesoporous alumosilicate (surface area 100 m^2/g, pore size 10 nm, grain size 0.4 mm) was used as an adsorbent for drying the wet air (relative humidity ~99 %) in the vacuum swing adsorption regime. Prior to VSA cycles, the adsorbent was calcined at 200 °C overnight and packed in a quartz cylindrical tube (length 0.2 m, i.d. 0.01 m) while hot. Transmission of quartz has some decrease in a range of 2.6–2.8 mm that falls in a sensitivity range of the used infrared camera 2.45–3.05 micron (Vainer 2000), however, the walls of the applied tube in a working spectral region were transparent enough to observe and quantify the thermal effects in the adsorbent, as demonstrated below.

The scheme of the experimental VSA setup is shown in Fig. 1. The wet air at ambient temperature (22 °C) under 10^5 Pa was supplied periodically through a 3-way valve to the adsorbent bed to fulfill an adsorption phase of the VSA cycle. During the adsorption phase the product gas passed through a back valve at the outlet of the bed. The volumetric rate of feed gas was 300 cc/s STP. In a certain time, the 3-way valve was switched to connect the adsorbent bed with the membrane vacuum pump. At this time the back valve closed allowing to reduce the pressure down to ~0.01 ati and thus to fulfill the desorpion phase of the VSA cycle. We tried 2 different ratios between adsorption/desorption duration, namely: regime 1 (adsorption 90 s, desorption 180 s), regime 2(adsorption 180 s, desorption 90 s).

The spatial temperature propagation was visualized and acquired by means of FPA-based infrared camera TKVr-IFP/SVIT manufactured at A.V.Rzhanov Institute of Semiconductor Physics SB RAS (Novosibirsk, Russia). This camera is equipped with the 128 × 128-pixel InAs infrared detector (Kurishev et al. 1998; Vainer 2004). The camera provided 100 fps frame rate acquisition and 0.027 °C temperature sensitivity. The infrared cameras of this type were used earlier in precise bio-medical (Vainer 2005) and physical (Vainer 2008) studies.

It is known that to monitor relatively high temperature catalytic reactions accompanied with large shifts of temperature by means of IR thermography one should consider the emissivity differences (Loskyll et al. 2012).

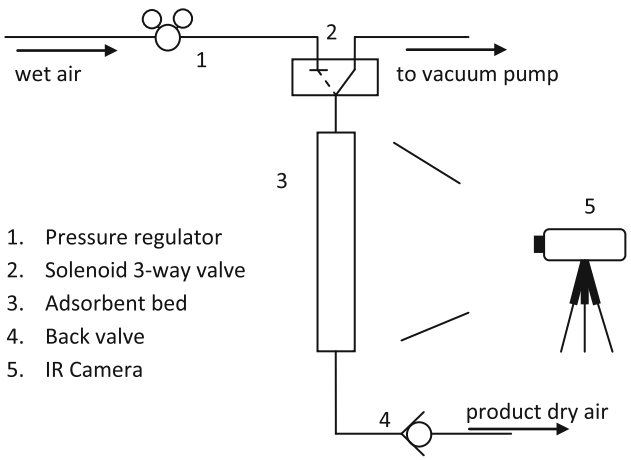

Fig. 1 Scheme of VSA experimental setup coupled with IR camera

The temperature shifts in our experiments did not exceed 15 K. Thus, the possible influence of adsorbent surface emissivity was assumed to be negligible.

During the experiments, the thermal imaging camera was mounted at the distance of 0.5 m from the adsorbent bed. Continuous recording of two-dimensional thermal images was performed. The obtained images were stored in the computer for further processing. To account the changes in the background during the long-term measurements, the detector was automatically periodically corrected.

3 Model

To simulate adsorption phase of VSA cycle we assumed non-adiabatic mass and heat transfer in a framework of Linear Driving Force (LDF) model, which is discussed elsewhere (Ruthven et al. 1994).

The model includes accounting mass balance:

$$\frac{u}{\varepsilon_b}\frac{\partial Y}{\partial z}+\frac{\partial Y}{\partial t}=D_L\frac{\partial^2 Y}{\partial z^2}-\frac{\rho_b R_g T_g}{\varepsilon_b P_{tot}}(1-Y)\frac{\partial \overline{q}}{\partial t} \tag{1}$$

$$\frac{\partial \overline{q}}{\partial t}=k_{LDF}(q^*-\overline{q}) \tag{2}$$

Temperature balance:

$$\frac{u}{\varepsilon_b}\rho_g C_{pg}\frac{\partial T_g}{\partial z}+\rho_g C_{pg}\frac{\partial T_g}{\partial t}=\lambda_L\frac{\partial^2 T_g}{\partial z^2}+\left(\frac{1-\varepsilon_b}{\varepsilon_b}\right)\frac{6h_{fs}}{d_s}(T_s-T_g)+\frac{4h_w}{\varepsilon_b d_r}(T_w-T_g) \tag{3}$$

$$\rho_p\left(C_{ps}+C_{pH2O}\overline{q}\right)\frac{\partial T_s}{\partial t}=(-\Delta H)\rho_p\frac{\partial \overline{q}}{\partial t}+\frac{6h_{fs}}{d_s}(T_g-T_s) \tag{4}$$

Adsorption equilibrium:

$$q^*=\frac{q_{\max}K(T_s)YP_{tot}}{1+K(T_s)YP_{tot}} \tag{5}$$

with the temperature dependence of interaction coefficient:

$$\ln\left(\frac{K(T_s)}{K(T_{ref})}\right)=\frac{Q}{R_g}\left(\frac{1}{T_s}-\frac{1}{T_{ref}}\right) \tag{6}$$

The starting conditions were chosen as

$$\begin{aligned} Y(z,0)&=0\\ \overline{q}(z,0)&=0\\ T_g(z,0)&=T_z(z)\\ T_s(z,0)&=T_z(z), \end{aligned} \tag{7}$$

and boundary conditions were as follows:

$$\begin{aligned} Y(0,t)&=Y_0\\ \overline{q}(0,t)&=0\\ T_g(0,t)&=T(0)\\ T_s(0,t)&=T(0) \end{aligned} \tag{8}$$

$$\begin{aligned} \frac{\partial Y(z=z_L,t)}{\partial z}&=0\\ \frac{\partial T_g(z=z_L,t)}{\partial z}&=0 \end{aligned} \tag{9}$$

The meaning and the values of the applied parameters are listed in Table 1. The following simplifying assumptions were made: the concentration of water vapor in the deeding air is low. Thus, the equation of the state of an ideal gas could be

Table 1 Basic model definitions

Y	Fluid phase molar fraction	kmol/kmol
$\overline{q}$	Grain averaged molar loading in adsorbed phase	kmol/kg
q^*	Equilibrium loading (H_2O/adsorbent)	kmol/kg
$q_{\max}$	Saturation loading (H_2O/adsorbent)	(0–0.01) kmol/kg
T_g	Gas phase temperature	K
T_s	Grain temperature	K
T_{ref}	Reference temperature, Eq. (5)	323 K
T_w	Inner wall temperature	298.15 K
z	Axial position	(0–0.225)m
t	Time	(0–240)s
R_g	Gas constant	8.314×10^3J/kmol K
u	Linear flow velocity	0.0645 m/s
ε_b	Bed voidage	0.4
P_{tot}	Total pressure in adsorber	101325 Pa
ρ_b	Bulk density	770 kg/m^3
D_L	Binary diffusion coefficient (H_2O/air)	1.4×10^{-5}м^2/c
k_{LDF}	Linear driving force constant	$(1–10)\times10^{-3}$s^{-1}
ρ_g	Gas density	kg/m^3
C_{pg}	Gas heat capacity	$(1.012–1.86)\times10^3$ J/kg K
λ_L	Heat transfer rate coefficient of air	0.0262 W/m K
d_s	Grain diameter	4×10^{-4}m
d_r	Inner diameter of adsorber	1×10^{-2}m
h_{fs}	Gas-grain overall heat transfer coefficient	1.7 W/m^2
h_w	Gas-wall overall heat transfer coefficient	1.4 W/m^2
ρ_p	Grain density	1200 kg/m^3
C_{ps}	Grain heat capacity	1.05×10^3 J/kg K
C_{pH2O}	Water heat capacity	76 J/kmol K
$K(T)$	Adsorption equilibrium constant	(0.00001–0.04)Pa^{-1}
ΔH	Enthalpy of water sorption	$6{,}250R_g$
Q	Water sorption heat	$-\Delta H$

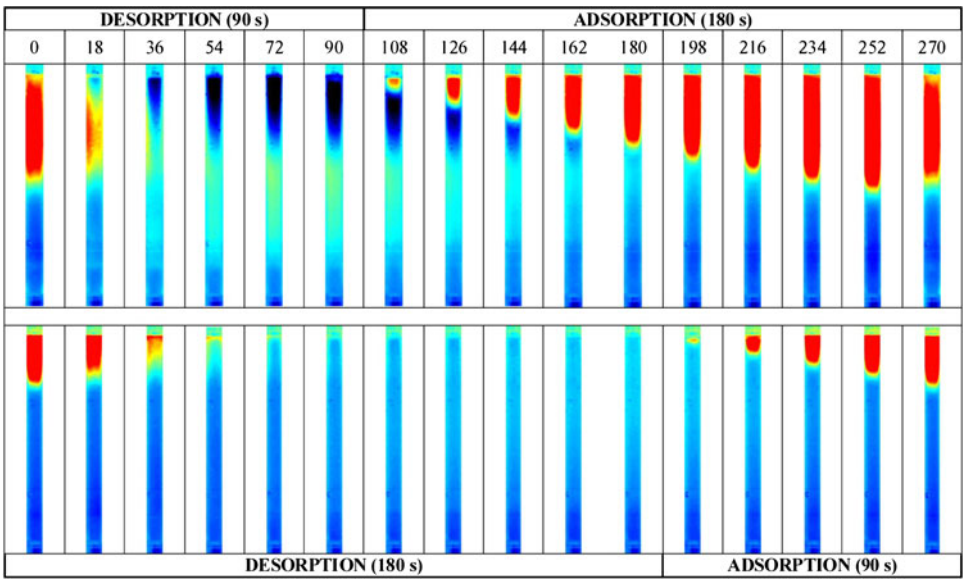

Fig. 2 2D thermal images of the adsorbent bed during VSA cycles (90 s desorption/180 s adsorption, *upper*) and (180 s desorption/90 s adsorption, *lower*), correspondingly

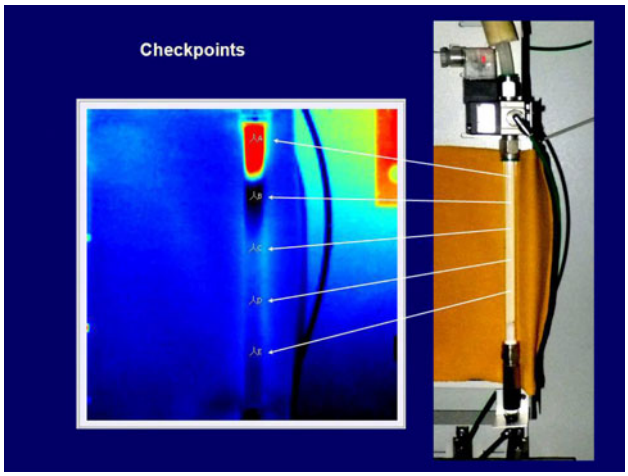

Fig. 3 Checkpoints selected in the adsorbent bed

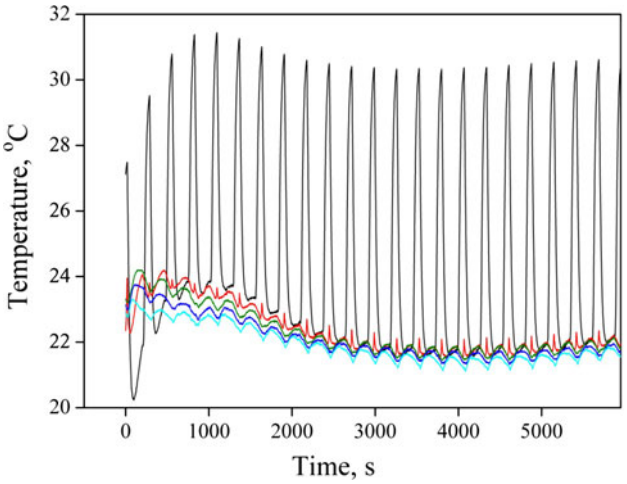

Fig. 4 Temperatures at the selected points in the bed for 90 s adsorption/180 s desorption VSA cycle. Color of curve and the associated checkpoint shown in Fig. 3: *black*—A, *red*—B, *green*—C, *blue*—D, *light-blue*—E

applied, the pressure drop through the bed is negligible, the linear flow rate is constant along the bed, the radial gradient in the adsorber is absent; the process is close to adiabatic (the heat exchange with the ambient is small).

The calculation of temperature profiles produced by the numerical solution of Eq. (1–4) with initial and boundary conditions (7–9) was fulfilled using the method of lines (approximation of differentiation operators to the space variable followed by the solution of ordinary differential equations). The total number of sampling points along the spatial coordinate derivatives was 250. To compare the simulated profile with the experimental, the initial temperature distribution along the bed was taken from the experiment at the beginning of the adsorption phase of the VSA cycle. To provide the simulation we used MATMOL 1.4 (http://matmol.org) package and MATLAB 2012a software.

4 Results and discussion

Figure 2 shows the images of a heat wave moving down during the adsorption phase and up during the desorption phase of the VSA cycle when stationary conditions were achieved. The images were extracted from the IR "movie" at intervals of 18 s: thus, 15 images in a row correspond to successive duration of the cycle. The first and the last images correspond to the beginning of the desorption and the end of adsorption phase, correspondingly. Red color corresponds to the patterns having the temperature exceeding ambient, which is while dark blue color corresponds to the temperatures lower than ambient.

Temperature maps provide full information on heat propagation in the adsorbent bed. However, to analyze the obtained results it is more convenient to split them into parts. For example, one can select several points (checkpoints A–E, Fig. 3) along the bed and follow the time dependence of temperature in these points. Corresponding temperature profiles in these points during prolonged VSA cyclic separation operation are shown in Figs. 4 and 5. One can estimate the characteristic time that is necessary to reach stationary regime from these data. In both cases it was found to be at the level of 3,000–4,000 s, or 10–15 cycles.

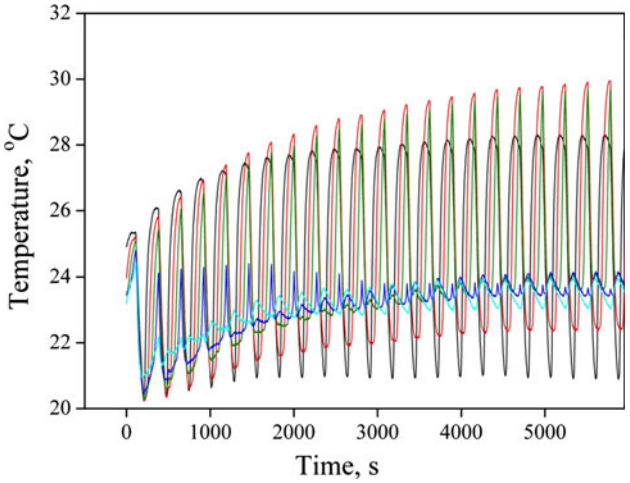

Fig. 5 Temperatures at the selected points in the bed for 180 s adsorption/90 s desorption VSA cycle. Color of curve and the associated checkpoint shown in Fig. 3: *black*—A, *red*—B, *green*—C, *blue*—D, *light-blue*—E

Figures 6 and 7 show the propagation of temperature profiles along the bed during both adsorption and desorption phases after the stationary conditions of the VSA cycle were reached. During the adsorption stage, a rapid increase of the pressure (probably in a mode similar to shock wave) occurs and the adsorber is quickly filled with air. Then the adsorption of water vapor starts and the corresponding temperature wave forms due to heat generation caused by the adsorption of water vapor. The observed magnitude of the temperature increase is low and does not exceed 8 °C. Temperature wave propagates uniformly in time and its rate is much lower than the linear velocity of the gas flow. During desorption there is a rapid drop of pressure in the adsorber followed by the desorption of water vapor from the bulk of the adsorbent. Desorption is accompanied by

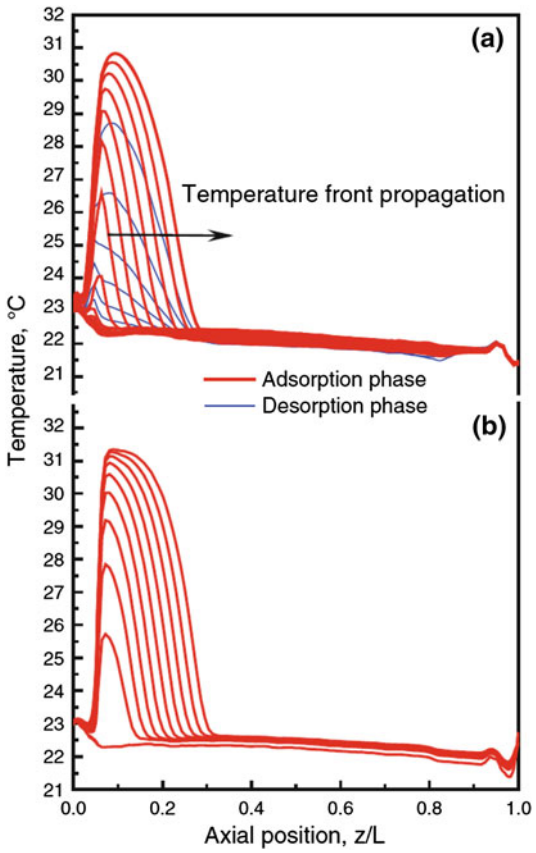

Fig. 6 Co-axial temperature profiles for 90 s adsorption/180 s desorption VSA cycle: **a** experiment, **b** simulation

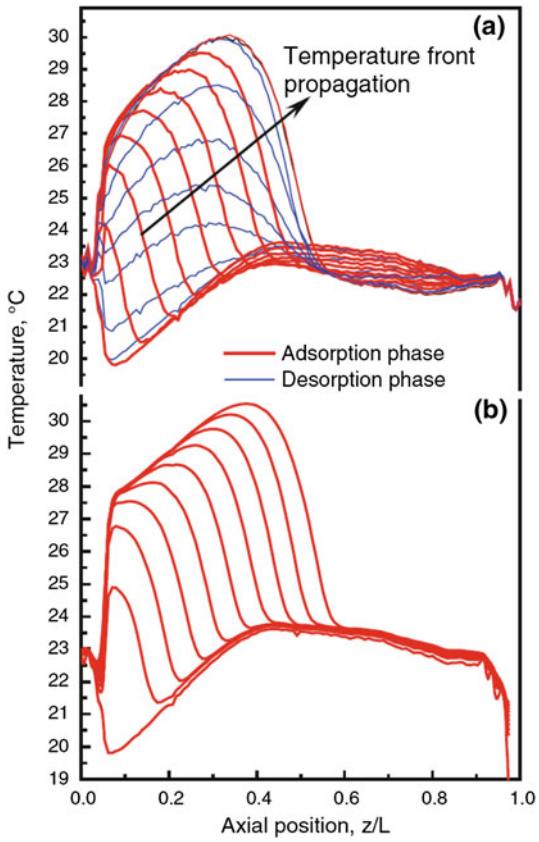

Fig. 7 Co-axial temperature profiles for 180 s adsorption/90 s desorption VSA cycle: **a** experiment, **b** simulation

the expected absorption of heat and cooling of the granules. In contrast to the adsorption phase, the temperature front in the bed does not appear; the temperature profile in the bed uniformly "sags" throughout its length.

Modeling of the adsorption step shows that the model (1–4) satisfactorily describes the dynamics of heat transfer in the bed (Figs. 6, 7): The appropriate choice of the model parameters gave the same temperature profile, which was observed experimentally.

The obtained results show the possibility of application of the model (1–4) to describe the propagation of the temperature profiles along the adsorbent bed. This fact shows that the adopted model can be used to describe the flow of small impurity adsorption in the gas flow.

The desorption rate of the gas flow out from adsorbent grains varies in time; so, model (1–4) cannot be applied to simulate desorption. The possible extension of this model is the subject of the on-going research.

5 Conclusions

This research demonstrates the possibility of application of IR thermography for the contact free real-time acquisition of 2D images that reflect propagation of temperature during cyclic adsorption–desorption experiments. Temperature sensitivity and the frame rate acquisition of the applied IR camera are high enough to obtain detailed data that describe behavior of VSA drying process. IR thermography allows obtaining information on actual temperature propagation rate, time that is necessary to achieve stationary regime of gas separation, the part of the adsorbent bed from the whole bed length which participates in stationary separation even when no adsorbate breakthrough is observed at the outlet of the bed. The obtained experimental data correlates well with LDF non-adiabatic model of mass and heat transfer.

Acknowledgments This research was supported by the Russian Foundation for Basic Research (grant No. 11-03-00900). The authors acknowledge Supercomputing Center of the Novosibirsk State University for providing the access and technical assistance.

References

Berkessel, A., Ashkenazi, E., Andreae, M.R.M.: Discovery of novel homogeneous rare earth catalysts by IR-thermography: epoxide opening with alcohols and Baeyer–Villiger oxidations with hydrogen peroxide. Appl. Catal. A **254**, 27–34 (2003)

Guerrero-Lemus, R., Martinez-Duart, J.: Hydrogen Production in Renewable Energies and CO_2, pp. 89–111. Springer, London (2013)

Jolly, J., Pavageau, B., Tatibouet, J.-M.: Time-resolved IR thermographic detection of gaseous molecules adsorption on oxide supports. Quantit. InfraRed Thermogr. J **8**, 129–137 (2011)

Khalighi, M., Farooq, S., Karimi, I.A.: Nonisothermal pore diffusion model for a kinetically controlled pressure swing adsorption process. Ind. Eng. Chem. Res. **51**, 10659–10670 (2012)

Kurishev, G.L., Kovchavtzev, A.P., Vainer, B.G., et al.: Medical infrared imaging system based on a 128 × 128 focal plane array for 2.8–3.05 microm spectral range. Optoelectronics, Instrumentation and Data Processing (Autometria) **4**, 5–10 (1998)

Loskyll, J., Stoewe, K., Maier, W.F.: Infrared thermography as a high-throughput tool in catalysis research. ACS Comb. Sci. **14**, 295–303 (2012)

Lou, H., Miyajima, H., Dong, F., Kodama, A., Goto, M., Hirose, T.: Experimental study of thermal phenomenon in PSA air dehumidification. Sep. Purif. Technol. **17**, 65–75 (1999)

Ruthven, D.M., Farooq, S., Knaebel, K.S.: Pressure Swing Adsorption. VCH Publishers Inc., New York (1994)

Vainer, B.G.: Limitary operation conditions affecting CID short-wave infrared detector performance. Meas. Sci. Technol. **15**, 821–830 (2004)

Vainer, B.G.: FPA-based infrared thermography as applied to the study of cutaneous perspiration and stimulated vascular response in humans. Phys. Med. Biol. **50**, R63–R94 (2005)

Vainer, B.G., Mel'gunov, M.S., Ayupov, A.B., Fenelonov, V.B.: Real-time thermal imaging and quantitative characterization of adsorption-desorption processes in zeolites and silica gels. In: 11th International Conference on Quantitative InfraRed Thermography, QIRT 2012, 11–14 June, 2012, Naples-Italy. E-Book Proceedings (2012-ISBN 9788890648441)—Italy: University of Naples, 2012.—ID-252 (9 pp) (2012)

Vainer, B.G.: Focal plane array based infrared thermography in fine physical experiment. J Phys. D: Appl. Phys. **41**, 065102 (12 pp) (2008)

Vainer, B.G.: Narrow spectral range infrared thermography in the vicinity of 3 μm operating wavelength. In: D. Balageas, J.-L. Beaudoin, G. Busse, and G.M. Carlomagno (eds) Quantitative InfraRed Thermography 5, Eurotherm Seminar 64, QIRT'2000, Reims, France, July 18–21, 2000. Proceedings, pp. 84–91. France: UTAP URCA, (2000)

Vainer, B.G., Mogilnikov, K.P., Romanov, S.I., Ayupov, A.B., Mel'gunov, M.S., Fenelonov, V.B.: Infrared thermography and ellipsometry investigations of vapour adsorption on zeolites, silica gels and porous films. In: Modern Trends in Science: New Opinion// Intern. Virtual Scientific-Practical Conf., November 29, 2011. Proceedings (9 parts). Part 7. Tambov: TROO "Business-Science-Society", 2011, pp. 24–28 (163 pp.). (in Rus.) (2011)

Voss, C.: Applications of pressure swing adsorption technology. Adsorption **11**, 527–529 (2005)

Wilcox, J. (2012) Adsorption in Carbon Capture, pp. 115–175. Springer, US